High speed, intermediate resolution, large area laser beam induced current imaging and laser scribing system for photovoltaic devices and modules

Adam B. Phillips,[1] Zhaoning Song,[1] Jonathan L. DeWitt,[1] Jon M. Stone,[1] Patrick W. Krantz,[1] John M. Royston,[1] Ryan M. Zeller,[1] Meghan R. Mapes,[1] Paul J. Roland,[1] Mark D. Dorogi,[2] Syed Zafar,[2] Gary T. Faykosh,[2] Randy J. Ellingson,[1] and Michael J. Heben[1]

[1]*Wright Center for Photovoltaic Innovation and Commercialization (PVIC), Department of Physics and Astronomy, University of Toledo, Toledo, Ohio 43606, USA*
[2]*Willard and Kelsey Solar Group, Perrysburg, Ohio 43551, USA*

We have developed a laser beam induced current imaging tool for photovoltaic devices and modules that utilizes diode pumped Q-switched lasers. Power densities on the order of one sun (100 mW/cm^2) can be produced in a ~40 μm spot size by operating the lasers at low diode current and high repetition rate. Using galvanostatically controlled mirrors in an overhead configuration and high speed data acquisition, large areas can be scanned in short times. As the beam is rastered, focus is maintained on a flat plane with an electronically controlled lens that is positioned in a coordinated fashion with the movements of the mirrors. The system can also be used in a scribing mode by increasing the diode current and decreasing the repetition rate. In either mode, the instrument can accommodate samples ranging in size from laboratory scale (few cm^2) to full modules (1 m^2). Customized LabVIEW programs were developed to control the components and acquire, display, and manipulate the data in imaging mode. *Published by AIP Publishing.* [http://dx.doi.org/10.1063/1.4962940]

I. INTRODUCTION

Laser beam induced current (LBIC) measurements, which spatially resolve the current collection in solar cells, have proven to be very helpful for characterizing devices. In the LBIC measurement, the beam is moved relative to the sample while the photogenerated current is detected and recorded. The resultant current maps can be used to identify nonuniformities in layer thicknesses, localized shunts, as well as cell interconnection issues.

Currently reported LBIC systems exhibit one or more limitations. Early instruments measured the current as a laser beam was translated across a fixed sample with a technique based on the use of rotating mirrors and a unitary telescope.[1–3] Samples could be examined rapidly with laser spots ranging in size from 2 to 25 μm, but the scan sizes were limited to ~10 cm × 10 cm due to the size of the telescope's lens, and the resolution was limited to 512 × 512 data points by the electronics that were available. Advances in the development of precision linear motion stages in the late 1980s and early 1990s permitted an approach where the laser beam was fixed, while the sample was translated in two orthogonal dimensions.[4] Although small spot sizes could be achieved (~3 μm), samples sizes were limited by stage travel limitations, and the imaging speed was limited by the speed at which the sample could be moved and the data acquisition rates.

Matson *et al.*[5] introduced a new approach that employed galvanostatically controlled mirrors that offered rapid scanning over large areas (up to 4 m^2) with an unfocussed laser beam. However, the image resolution was limited to 1000 × 1000 points and the time to acquire the image was slowed by

the electronics that were available. Acciarri *et al.*[6] pushed the data point density to higher values for smaller samples (10 × 10 cm), but the speed of data acquisition was still limited by the time response of the lock-in amplifier that was employed. Vorasayan increased the size of the scans to 30 cm × 30 cm[7] and 120 cm × 120 cm[8] using beams that were ~1 mm and 0.41 mm wide, respectively. These efforts demonstrated a good balance between the size and rate of acquisition of the scan while maintaining a useful image resolution.

Even with recent advances, many LBIC systems still use relatively slow mechanically chopped optical beams and phase sensitive detection to generate and collect the photocurrent data. Thus, the overall data acquisition rate is typically slow and there is still a trade-off between scan area, spatial resolution, and measurement time. For example, Krebs and Jørgensen[9] reported in 2014 a configuration that allows for rapid scan of areas 30 cm × 30 cm by using a storage oscilloscope, but the size of the storage data buffer introduces a new compromise between the size of the scanned area and the spatial resolution at which the data may be obtained.

Another limitation in LBIC systems is that the continuous wave (CW) lasers that are typically used operate at powers that are too high for small spot, moderate resolution scanning. For example, a relative weak 1 mW CW laser focused to a 40 μm spot would present a power density of ~80 W/cm^2 which is 800 times greater than the power density of 1 Sun at the surface of the Earth (a standard AM1.5G solar spectrum has a power density of ~100 mW/cm^2). Many photovoltaic materials and devices are damaged under such high light intensities and, even without damage, the physics of carrier generation and recombination under such high injection

conditions are typically very different from behaviors under 1 Sun conditions. Of course, the light intensity could be reduced by employing larger spot sizes, but the spatial resolution would be commensurately reduced. Neutral density filters could also be employed, but operation of a Q-switched laser at high repetition rates, as is done here, affords an alternative method to achieve low power densities.

Here, we present an LBIC system that uses diode-pumped Q-switched lasers as the light source. By operating the laser at a frequency of 600 kHz with diode pump currents that are just sufficient to produce lasing, we are able to illuminate our sample with a 40 μm wide beam at total average power of ~2 μW, giving rise to an illumination power density of ~100 mW/cm^2, which is the power density in the standard AM1.5 solar spectrum. Additionally, by placing the galvanostatically controlled steering optics ~1 m above the sample and utilizing high speed data acquisition techniques we are able to measure samples up to 60 cm × 60 cm at full 40 μm resolution at a scan rate of 1 m/s. The instrument affords a further advance in the compromise between scan size, scan speed, and resolution with advanced electronics and software such that movies of fast, real-time degradation of photovoltaic cells can be made by LBIC.[10] Finally, an additional benefit associated with using a Q-switch laser is that this system can be easily converted into a scribing system simply by increasing the diode current and decreasing the frequency.

II. OPTICS AND OPTICAL CONTROLS

Figure 1 shows the layout of the apparatus. The system consists of a 4′ × 8′ optical table (Newport RS4000) on which a second 4′ × 4′ optical table (Newport SG-44-4) is mounted with 83 cm long aluminum posts (80/20 Inc., Model 3030). The second, upper optical table was specifically designed with a rectangular cut-out in the center (15 cm × 56 cm). The second table holds the lasers and optics for beam management, focusing, and steering, while the lower table holds the samples. The line of sight for the laser beam through the rectangular cut-out allows for rapid, large area scanning through the second table's rectangular hole. The upper and lower tables comprise a rigidly connected system that limits vibrations from interfering with the data collection and scribing processes. The entire system may be floated to further reduce vibrational coupling.

To achieve the rapid and accurate scanning, two orthogonal galvanostatic controlled mirrors (General Scanning, Inc. HPLK series) are coupled with a z-focus lens to control the beam location. The mirrors have a maximum rotation speed of 60°/s, resulting in beam speeds greater than 1 m/s on the surface of the device. The addition of the z-focus lens, which is coordinated with the mirror motion using the control system (Cambridge Technology EC1000), maintains the beam focus on the sample surface over scanning distances greater than 60 × 60 cm.

To maximize the utility of the system, three Spectra-Physics Nd:YAG diode-pumped lasers with wavelengths of 1064 nm, 532 nm, and 355 nm can be used to excite materials differently depending on the band gap and absorption coefficient. The 532 nm wavelength is most often used because the photon energy (2.33 eV) is above the band gap for most solar cell materials. The 1064 nm wavelength laser can be used for Si and is particularly useful for probing the performance of bottom cells in, e.g., perovskite/Si, tandems. In this case, additional light sources with appropriate filters can be readily included to provide needed light biasing.

Figure 2 shows the average output power of the 532 nm wavelength laser as a function of the laser diode pump current and Q-switch repetition rate. The right axis shows the average power density for a 40 μm diameter spot size. We have found that the laser output power is relatively stable over extended periods of time at low diode current and high repetition rates. Each laser has its own set of steering and focusing optics, and, prior to reaching these, the beam is passed through a beam expanding element (Figure 1) to enable production of a 40 μm diameter spot at the sample surface.

The raster pattern that the mirrors follow can be defined in Cambridge Technology's Scan Master Designer (SMD) software. The software allows for any pattern to be the input
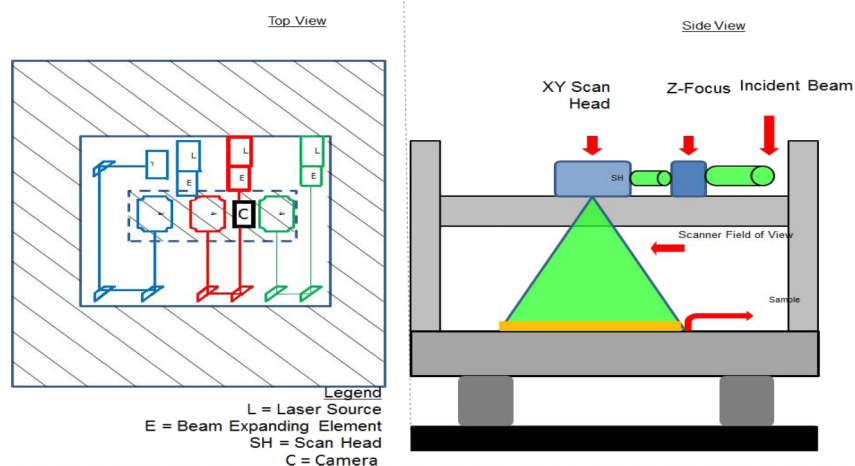

FIG. 1. Schematic diagram of laser setup with the locations of the optics and the galvanometers. The top view shows the location of the optics associated with each laser and camera, while the side view shows the relative sample location and field of view.
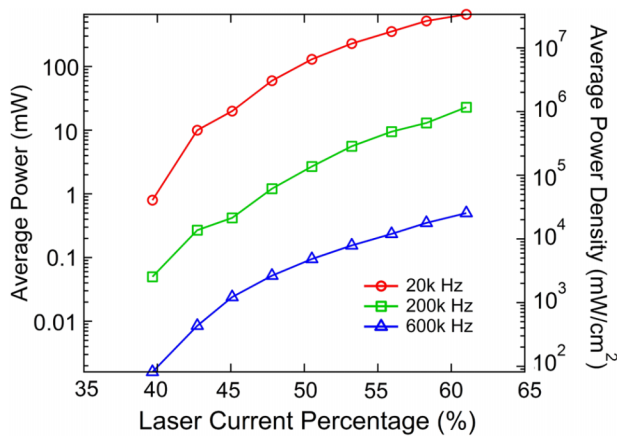
FIG. 2. Average power of the frequency doubled Nd:YAG laser as a function of laser diode current percentage for a variety of laser repetition rates. The right axis shows the average power density for a spot size on the surface of our samples with diameter of 40 μm.

and sent to the optics via the control board. The beam speed and number of times a pattern is repeated are also inputs in the software. SMD communicates with the laser control software, JWin, so that laser selection and the laser diode current maybe controlled from a single user interface. A camera is coupled to SMD to import an image to define the sample's location in the system's coordinate system. This allows the programmed beam pattern to be directly applied to the sample without alignment or the use of a test device. The lasers' beam positions were adjusted so that the home positions as defined in the software were coincident.

III. LBIC MEASUREMENT SYSTEM

A. Hardware

The samples are loaded onto a stage and rail system that can accommodate a wide range of sample geometries and sizes. The stage consists of a 15 cm × 15 cm machined Al platform, which can accommodate common samples sizes (e.g., 2.5 cm × 3.8 cm and 2.5 cm × 7.5 cm) and an opening with a movable side that can be adjusted to hold samples up to 12.5 cm × 12.5 cm. The stage height is fixed on a set of rails such that there is sufficient room behind the sample to make connections at the back of devices fabricated in the superstrate configuration. The stage itself is sufficiently rigid to allow mounting of probes to make connections to the front of the devices prepared in the substrate configuration. The stage can be removed, and full panels can be loaded directly onto the support rails.

To provide LBIC measurements of cells in a thin-film monolithically integrated module, connection to the back contacts of two adjacent cells is made using pogo pins spaced according to the width of the cell. These pin contacts may be translated in two orthogonal dimensions using two stepper motors and screw drives. For a module fabricated in the superstrate configuration (e.g., CdTe), one stepper motor can be used to engage (disengage) the probe head pins with the cells by moving up (down). The positive engagement (disengagement) condition can be determined by measuring

the electrical continuity in the cell. The stepper motors and associated current/voltage measurements are controlled using a LabVIEW virtual instrument (VI). The second translation axis can be used to move the pins from cell to cell after measurement of a given cell has been completed. With this approach, 40 μm resolution LBIC images may be obtained from full panels with minimal user interaction.

The current data may be collected using a current amplifier (e.g., Keithley 428) and a high speed data acquisition device (DAQ; e.g., National Instruments NI USB 6251). Alternatively, a high speed source meter (e.g., Keithley 2601) may be used. The former approach is a two-point measurement in which lead resistances may be important, while the latter allows four point measurements and also permits measurement as a function of applied bias. In particular, it should be noted that by setting the source meter for open circuit conditions, the laser beam induced voltage can also be measured to avoid resistance losses.

B. Data acquisition software

To obtain accurate and high resolution data, the instrument must allow precise control over (a) the translation of the beam across the sample and rapid return to a starting position, (b) the coordination between the start of data acquisition and laser illumination, (c) the timing between each data point collected, and (d) the required time to transmit the data from the buffer on the data acquisition board to the computer. Three separate pieces of software are used in coordination to enable the overall data acquisition. These are JWin, SMD, and a custom developed LabVIEW data collection VI.

JWin and SMD are used to control the laser and the laser beam location on the sample. While SMD can communicate with the JWin software, the laser repetition rate cannot be controlled. Consequently, the repetition rate must be set to the appropriate repetition rate (600 kHz for measurements) in the JWin software. SMD controls every other aspect of the laser and the laser beam location. After the sample is loaded and appropriately connected for the measurement, the image of the chamber is loaded into the SMD interface. Then, the beam pattern may be defined as array of lines with a fixed spacing between the lines. The laser power, scan speed at which the laser beam should be moved across the sample, and the return speed (to position the beam for the start of a next line) are defined in the SMD software.

The LabVIEW VI coordinates the data collection with the laser beam movements. The length and total area of the scan and the space between raster lines are entered to define the workspace in the software. Next, the power to the laser is turned on, but the laser diode current is held at zero. The programmed scan is then activated in SMD, and the rastering (scanning and blanking) process is begun. A LabVIEW VI is then activated to record the exact time that the laser is on by reading the transistor-transistor logic (TTL) output of the laser status with one of the DAQ's 16-bit analog to digital ports. This information is then used to configure the DAQ sample rate or the Keithley 2601 power cycle and the sample rate. To maximize the speed of the measurement, the data are stored in the instrument buffer and uploaded to the computer as

the mirrors move the beam to the starting position of the next line. Data are transmitted from the Keithley 2601 in binary and converted to decimal values before writing to the file. Research scale device measurement is saved in a single file, while LBIC data for each cell of a module are saved in a single file and later constructed into an image of the entire module.

As previously mentioned, LBIC measurement on modules use a two-pin connector to contact each cell in the module. Therefore, the software must determine when the connector needs to move to the next cell. In the case of modules, each cell is scanned individually by designating a scan area that covers the cell. When the scan is complete, the instrument waits a sufficient time to allow the two-pin connector to be moved to form connections with the next cell. Once the connection is remade, the scan of the subsequent cell can commence. The data are written to a file line by line, and the data file is closed when the scan of the cell is complete. A new file is opened and used for the next cell. This process is continued until the measurement is complete. Half of a 60 × 120 cm module can be imaged with the current apparatus without user interaction.

C. Data analysis software

While the data files can be loaded into any analysis software, the file size for the image of a full panel is large (∼1 GB) and may be too cumbersome for many programs. As a result, we developed a LabVIEW VI to handle the large data files generated during these measurements. An additional stitching VI was developed to concatenate the LBIC files for each cell to create two half panel files, then to mirror the data set of the second half of the panel, and combine it with the data from the first half to generate the full panel file.

This analysis VI loads the file and allows for data manipulation and calculations over cross sectional slices or areas of the data. The data are displayed on the monitor at a lower resolution to allow an overview of the entire area. As an area is expanded, the resolution of the image increases to allow finer detail to be observed. The average, standard deviation, maximum, minimum, and other statistics can be obtained using a cross-sectional slice of the data.

IV. RESULTS

Figure 3(a) shows a quantum efficiency map of a perovskite solar cell measured using 532 nm excitation. The measured LBIC is converted to quantum efficiency by measuring the LBIC from a reference cell at the same time

the sample is measured. Since the quantum efficiency at 532 nm is known for the reference cell, the LBIC data can be converted into quantum efficiency data. LBIC has been a powerful tool for perovskite samples because it shows that even good cells have non-uniformities in the current collection. Figure 3(b) shows a histogram plot of the quantum efficiency for the cell shown in Figure 3(a). The shape and breadth of the histogram plot can provide quantitative information about the uniformity of the current collection over the device area and often indicates the quality of the device. The spatial mapping of the quantum efficiency comments on the origins of limitations in the overall device performance and can also be used to image degradation processes.[10]

To demonstrate the wide range of sample sizes capabilities, the LBIC map of a full sized (60 cm × 120 cm) CdTe module is shown in Figure 4. The panel was formed in the typical device stack and was an early product of a new manufacturing process. Each half of the panel was connected in series, and the two halves were connected in parallel. For this measurement, the panel was not encapsulated and the individual cells were accessible. Each cell was individually connected into the measurement circuit using the moveable two-pin connector described above. The measurement was obtained using a laser wavelength of 532 nm. After measuring each cell, the data were combined to form a single file and loaded into the analysis VI. As seen in the figure, half of the panel performed poorly due to either interconnection or shunting issues. Note that the movable two-pin measurement method on individual cells avoids the need to make the cell under examination the current limiting cell,[8] as is required for LBIC of modules via current measured through the external leads. The 40 μm resolution of the LBIC measurement also allows for identification of process nonuniformities that may be present. For example, the yellow square in Figure 4(a) shows a number of features that traverse across several cells. Figure 4(b) shows the expanded view of this region. Because these features persist across a number of cells, they are likely caused during the deposition processing. Results like these indicate how LBIC measurements can be a valuable tool at the manufacturing level to not only identify bad cells but to help identify processing issues.

The results presented here provide a demonstration of the flexibility of the LBIC system, but are not a comprehensive demonstration. With two additional laser wavelengths, the depth of the devices can be probed. For example, the 355 nm light can be used to investigate the CdS layer of the devices, or the 1064 nm wavelength can be used to probe bottom cells of tandem devices. Intermediate size samples or mini-modules can also be accommodated in this system.

V. SCRIBING

An advantage of using a pulsed laser for LBIC measurements is that it can be converted into a scribing system simply by increasing the diode current and decreasing the repetition rate. Scribing is important in research scale devices to define the device area for evaluation purposes. This can be achieved by scribing a contact layer and the active material, when necessary, after a complete stack is deposited.
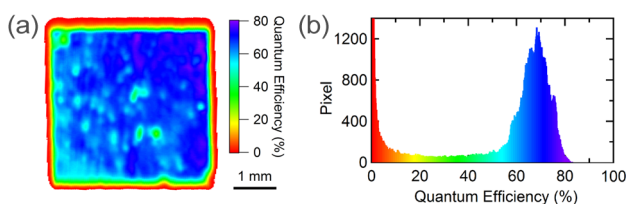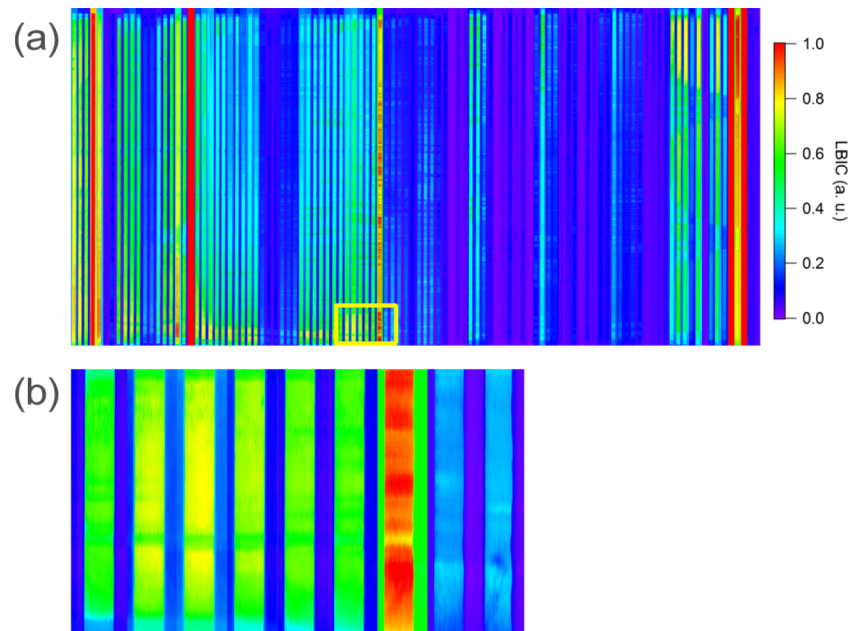

FIG. 3. (a) Quantum efficiency map of a perovskite solar cell. The LBIC measurement is converted to quantum efficiency using a reference device. (b) Histogram plot of quantum efficiency.

FIG. 4. (a) LBIC measurement of a full 120 cm × 60 cm panel from a commercial partner. (b) Expanded view of the yellow box in (a) that shows a reduced LBIC value over several cells.

Using our standard sample stage, and a high-efficiency particulate air (HEPA) filter vacuum system placed near the sample to collect scribing debris, we have scribed a variety of materials using parameters closely following those in the literature.[11–14] The 0.085 cm^2 cells shown in Figure 5(a) were prepared by scribing a single 25 mm × 25 mm solar cell using the frequency doubled Nd:YAG (532 nm) laser. The scribing parameters were the following: beam translation speed on sample was 500 mm/s; the average power was 700 mW; the beam size was ~40 μm; the laser repetition frequency was 20 kHz; and the peak pulse power was 5.5 kW. The latter quantity was derived from the average power, the pulse repetition rate, and the measured pulse width. The laser beam was incident upon the film side of the stack, and the scribe pattern was not repeated. These parameters result in complete removal of the metal back contact and partial removal of CdTe layer. A line defect was also scribed into the sample for imaging purposes (the lower right cell in Figure 5(a)). Figure 5(b) shows the LBIC image of the same sample.

VI. SUMMARY

A Q-switched laser based LBIC system is presented. By using a high repetition rate and low diode current, average power on the order of 0.01 mW (100 mW/cm^2 for a 40 μm spot size) is achievable. Three variable power lasers are incorporated to provide flexibility to the system. By controlling the beam location through overhead mirrors, the system is capable of performing these tasks at high speeds. The system and sample holder were built to accommodate a wide variety of sample sizes ranging in size from full panels to small research scale devices. LabVIEW software was developed to interact with commercial software to allow ease of operation, complete control, and high speed data acquisition. The combined movies of fast, real-time degradation of photovoltaic cells can be made by LBIC.[10] An advantage of using Q-switched lasers is that the system can be converted into a laser scribing system simply by increasing the diode current and decreasing the repetition rate.
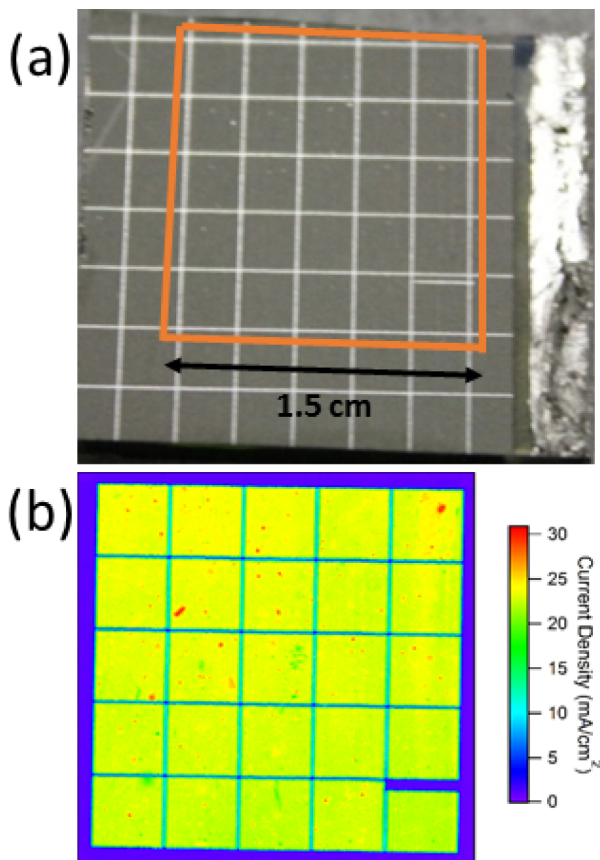

FIG. 5. (a) Photograph of a research scale device after scribing. The box indicates the samples that were measured. (b) LBIC measurement displaying the J_{SC} calculated using beam size and the light intensity.

ACKNOWLEDGMENTS

[1] D. E. Sawyer and H. K. Kessler, IEEE Trans. Electron Devices **27**, 864 (1980).

[2] S. Damaskinos, Sol. Cells **26**, 151 (1989).

[3] A. C. Ribes, S. Damaskinos, H. F. Tiedge, A. E. Dixon, and D. E. Brodie, Sol. Energy Mater. Sol. Cells **44**, 439 (1996).

[4] J. Bajaj and W. E. Tennant, J. Cryst. Growth **103**, 170 (1990).

[5] R. Matson, K. Emery, I. Eisgruber, and L. Kazmerski, in *Proceedings 12th European Photovoltaic Solar Energy Conference* (H.S. Stephens & Associates, Amsterdam, The Netherlands, 1994), p. 1222.

[6] M. Acciarri, S. Binetti, A. Racz, S. Pizzini, and G. Agostinelli, Sol. Energy Mater. Sol. Cells **72**, 417 (2002).

[7] P. Vorasayan, T. R. Betts, A. N. Tiwari, and R. Gottschag, Sol. Energy Mater. Sol. Cells **93**, 917 (2009).

[8] P. Vorasayan, T. R. Betts, and R. Gottschalg, Meas. Sci. Technol. **22**, 7 (2011).

[9] F. C. Krebs and M. Jørgensen, Adv. Opt. Mater. **2**, 404 (2014).

[10] Z. Song, A. Abate, S. C. Watthage, G. K. Liyanage, A. B. Phillips, U. Steiner, M. Graetzel, and M. J. Heben, Adv. Energy Mater. 1600846 (2016).

[11] A. D. Compaan, I. Matulionis, M. J. Miller, and U. N. Jayamaha, in *Photovoltaic Specialists Conference, 1996, Conference Record of the Twenty Fifth IEEE* (IEEE, 1996), p. 769.

[12] A. D. Compaan, I. Matulionis, and S. Nakade, Opt. Lasers Eng. **34**, 15 (2000).

[13] C. Ferekides and J. Britt, Sol. Energy Mater. Sol. Cells **35**, 255 (1994).

[14] V. Ramanathan, L. A. Russell, C. H. Liu, and P. V. Meyers, Sol. Cells **28**, 129 (1990).